Aerodynamic experiments on DelFly II: unsteady lift enhancement

K.M.E. De Clercq
University of Cambridge, CB2 3EJ Cambridge, United Kingdom

R. de Kat, B. Remes, B.W. van Oudheusden and H. Bijl
Delft University of Technology, 2629 HS Delft, The Netherlands

ABSTRACT

In flapping wing motion it is expected that both the clap and peel mechanism and the occurrence of a leading edge vortex during the translational phase play an important role in unsteady lift generation. Furthermore, the flexibility of the wing foil is also considered of primary relevance. Particle image velocimetry measurements and simultaneous force measurements have been performed on the DelFly II flapping-wing MAV, to investigate the flow-field behavior and the aerodynamic forces generated. The PIV analysis shows a strong influx of air between the wings during the peel but no downward expelling jet during the clap. The force measurements reveal that the peel, as opposed to the clap, contributes significantly to the lift. The PIV visualization suggests the occurrence of a leading edge vortex during the first half of the in- and outstroke, which is supported by a simultaneous augmentation in lift. The early generation of a leading edge vortex during the flex cannot be assessed from the PIV images due to optical obstruction, but is likely to appear since the wing flexing is accompanied with a large increase in lift.

1 INTRODUCTION

Some students of the Delft University of Technology impressed upon both the jury and public at the EMAV '05 conference, demonstrating the first flapping wing MAV with vision based control, called DelFly. Although they didn't manage to complete the competition's mission, the DelFly was nominated as "Most Exotic Design". Since then, interest in flapping wings has greatly increased and flappers are no longer uncommon.

Research and development on DelFly has led to a series of flapping wing MAVs, wherein the technological challenge is to decrease the size, while keeping the flight performance constant. The wing shape and stiffness has been optimized based on a trial-and-error approach. A better understanding of the aerodynamics is necessary as a guideline to further development of DelFly.

Previous work on insect flight [1,2] provides some insight in the lift enhancement mechanisms involved with flapping wings. DelFly II differs from typical insects and birds in its wing configuration, flapping frequency and wing size, such that only a restricted similarity in flow-field behavior can be expected.

Email address: kmed2@cam.ac.uk

Figure 1: DelFly II in hovering flight

In this study a full-scale and non-simplified model of DelFly II is considered. The flow field around the wings was analyzed by particle image velocimetry (PIV) while simultaneous force measurements indicate the relative contribution of the visualized flow structures to the lift generation. The data obtained in this study will be evaluated with the objective to contribute to the understanding and subsequent improvement of the aerodynamic characteristics of DelFly II.

2 METHOD AND MATERIAL

2.1 Model

Experiments are performed on full scale DelFly II-wings. The wings and gearbox planform are integrated in the experimental set-up without the usual fuselage and tail. The two sets of wings are positioned symmetrically with respect to the fuselage plane at a dihedral angle ψ of 12º. The wing's semispan from root to tip is 14 cm and the mean chord length, the ratio of the wing surface to the wing span, is 7.3 cm. The flapping motion is controlled by a crank-shaft mechanism moving the leading edges, hinged in one point, in a single plane. The maximal stroke angle Φ is 48°. In [3], the design and construction of the DelFly wings as well as the wing's kinematics are discussed thoroughly.

The choice has been made to observe DelFly in hovering flight (figure 1) because the unsteady aerodynamic effects, which are hardly predictable but are especially interesting for lift enhancement, are assumed to dominate over the quasi-steady ones in hovering flight configuration. The wings were positioned with the stroke plane aligned horizontally and the experiments were performed in a large cubic test volume,

where the surrounding flow was stationary, to simulate the hovering flight modus. The mean wingbeat frequency was selected as 13 Hz, which resembles a typical flapping frequency necessary to sustain hovering flight. The Reynolds number ($\mathrm{Re} = \overline{c}U_r / \nu$) based on the mean chord length ($\overline{c} = 2r / AR$) and the mean wing tip velocity ($U_r = 2\Phi nR$) [4] is 14 674.

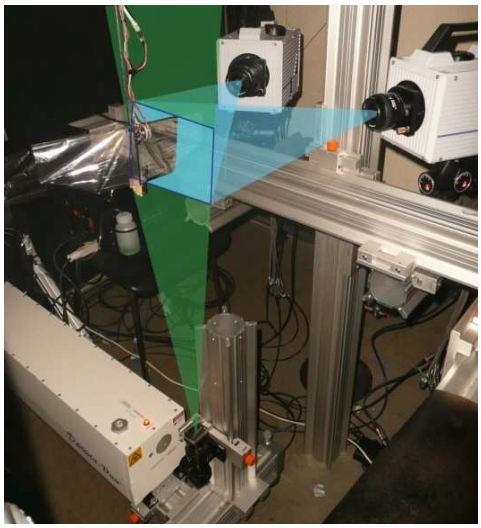

Figure 2: Experimental set-up for Stereoscopic Particle Image Velocimetry

2.2 *Flow visualization*

Stereoscopic particle image velocimetry has been used to visualize the three dimensional flow field around the flapping wings. The measurement plane is oriented parallel to the chord and perpendicular to the dihedral line at ¾ span (figure 2). Both cameras were placed symmetrically at an angle of 27° with respect to the dihedral line in an angular configuration. The parameters of the PIV apparatus are summarised in table 1.

field-of-view	202 (Δx) x 202 (Δy) mm^2
effective particle diameter	1 μm
pulse duration	200 ns
wavelength	527 nm
pulse separation time	200 μs
magnification	0.09
recording lens	35 mm
digital imaging resolution	5 pix/mm
$f_{\#}$-number	2.8
recording rate	1 kHz
interrogation window size	16x16 pixels

Table 1: PIV apparatus parameters.

The effect of background reflections on the images was reduced by subtracting the minimum intensity calculated over a range of (minimal 6) images where the wings are in approximately the same position. Calibration, data acquisition and data processing are carried out using Davis 7.3 software. A more elaborate discussion of the experimental set-up can be found in [5].

2.3 *Force Measurement*

Simultaneous force measurements provide information that may assist to interpret the contribution of visualized flow structures to the lift generation. The wings hang rigidly on a strain-gauge balance with two Wheatstone bridges, miniature sensors Q70x5x9-H with a capacity of 20 g (figure 3). Using a Picas V2.6.1 Multi-channel amplifier system the range was set from +40 g to -40 g. The vertical forces were measured and recorded at a sampling rate of 1000 Hz.

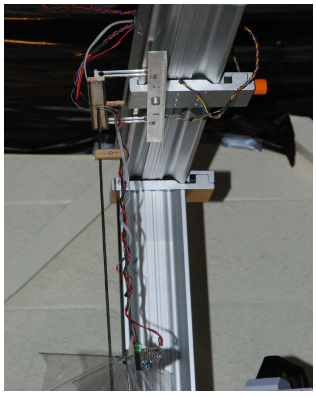

Figure 3: Strain gauge balance for measurement of lift force

3 RESULTS

3.1 *Wing trajectory*

As is the case in insect wings, the DelFly-wings are actuated at the wing base and the instantaneous shape of the wings is dictated by the interaction of aerodynamic, inertial and elastic forces. The deformations involve a variable angle of attack, favourable camber, spanwise bending and torsion, a leading edge heaving motion, wing-wing interaction and wing flexing during rotation. These kinematic features are known to have large influence on the aerodynamic forces generated during flight [6].

In figure 4, the wing shapes defined from visual inspection of the PIV recordings at ¾ spanwise position and at different stages of the cycle are sketched along with the non-dimensional time τ, which is the time instant divided by the cycle period. The in- and outward leading edge motions are shown in the upper and lower part of the figure, respectively. The figure clearly reveals the strong deformation of the flexible wing foil and leading edge.

Starting from the instant that the leading edge spars are closest together (τ = 0), the leading edge spars move apart at increasing velocity. The wing foil peels apart under high deformation. Weis-Fogh [7] states that two fluid dynamic effects are responsible for enhanced circulation during this type of motion, called the peel. The first is when the air is drawn in the low pressure region in the opening gap; and the second effect is that the proximity of the other wing with equal and opposite bound circulation inhibits the generation of a starting vortex.

At the end of this phase (label A), the trailing edges separate and the wings continue moving outward at a constant speed and angle of attack (label B). This part of the motion is named the translational phase.

Near the maximum wing stroke amplitude the leading edge spars decelerate (label C) and reverse direction while the trailing edges temporarily stay stationary: the wing flexes. When the leading edge further accelerates the foil unflexes (label D). This deformation largely resembles the flex mechanism as described by Ellington [8]. Due to this flex mechanism the leading edge has a larger velocity and vorticity

may shed into a separation vortex at the leading edge instead of the conventional starting vortex shed from the trailing edge. The bound vorticity is likely to roll up around the stationary trailing edge and shed as a combined starting and stopping vortex when the wing unflexes. This mechanism would provide the wing with a net circulation at the beginning of the following half stroke, which skips the gradual increase of lift due to the Wagner effect [9].

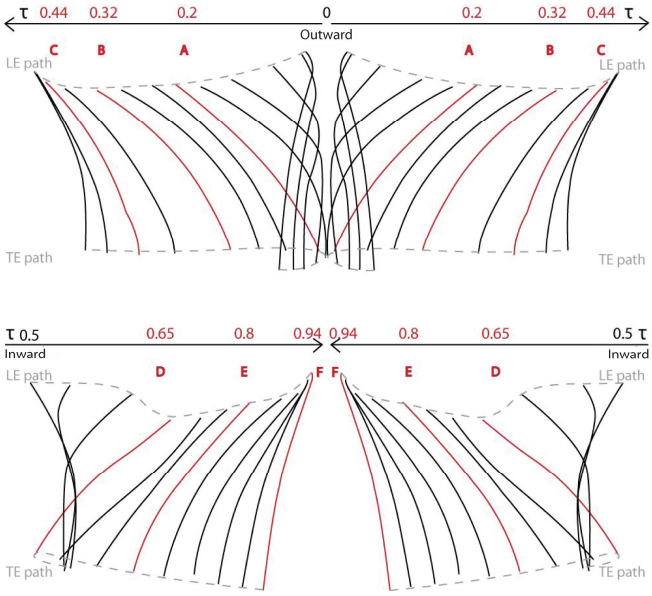

Figure 4: Schematic representation of the wing motion during one flap cycle *defined from visual inspection of the PIV recordings. In- and outward leading edge motion represented by upper and lower part respectively*

After having unflexed, the wing foil moves inwards (label E). Upon approaching each other, the leading edge spars decelerate causing the camber to decrease and the wing foils to clap together (label F). Weis-Fogh [7] argues that the clap mechanism produces a momentum jet augmenting lift. Instead of rigidly clapping the wings together, the clap is more akin to a reverse peel. Before the clap has been completed the leading edges have already started separating again, pulling the wing surfaces apart.

As to the vertical motion of the leading edge, it is observed that during the acceleration in the beginning of the translational stroke, the wing foil pulls tight and the leading edge is pulled downwards (label A and D). At the end of the stroke, tension is released and the leading edge moves back towards its original position (label C and F). The resulting wing tip trajectory with respect to the body is an elongated figure-of-eight shape. Thanks to the upward motion of the leading edge the foil is pulled tight during the rotation.

3.2 Force

The force variations with respect to the non-dimensional time are shown in figure 5, along with the flap angle and the labels A to F corresponding to the red wing sections in figure 4 and the flap angle. The error bars indicate the standard deviation of the force measurements over the complete measurement run (a minimum of 300 cycles).

The mean force over one cycle attains 0.21 N, which is largely sufficient to lift a DelFly II typically weighting 17 grams. Using the Osborne method to solve the blade element theory [10] for the mean lift coefficient a value of 2.39 is found.

$$(1) \quad \bar{C}_L = \bar{L} \Big/ \left(\frac{1}{2}\rho \int_0^R 2c(r) r^2 dr \cdot \frac{1}{T}\int_0^T \dot{\phi}^2 dt \right)$$

This high value for the mean lift coefficient shows that unsteady lift mechanisms are likely to be involved.

Figure 5 shows that the in- and outward translational strokes, defined as the part of the flapping cycle wherein the angular velocity of the wing's leading edge is constant, cover a similar time span. Comparing figure 4 to figure 5, it can be seen that the trailing edges have separated just before the start of the outstroke (label A) and that the angle of attack decreases significantly right after the outstroke has been finished (label C). A peak values occurs at 1/3 of the outstroke when the maximal force amounts to 0.69 N. The aforementioned definition of translation is more confusing in case of the instroke, since the direction of the wing's camber has not been reversed before the instroke starts (~0.45 τ). At 2/5 of the instroke, after the foil has unflexed (label D), a second peak force appears. This peak value of 0.56 N is 17% lower than the peak values attained during the outstroke. Notice that both peak forces appear near the neutral wing's position.

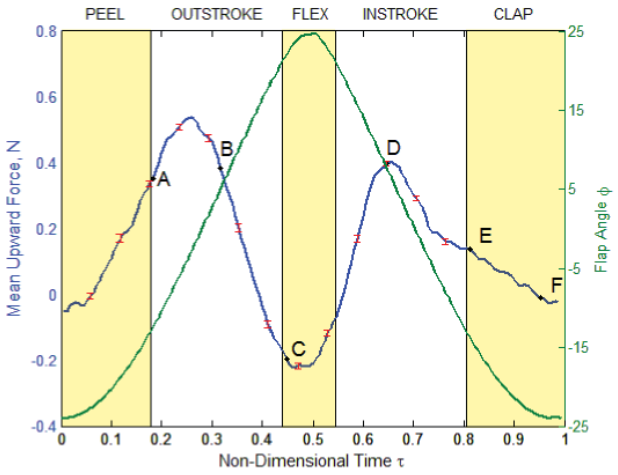

Figure 5: Upward force fluctuations and flapping angle during one flap cycle. *Error bars show standard deviation. Labels A to F correspond to the red-colored wing sections identified in fig. 4*

Complementary to the definition of translation, rotation is defined as the phase in which the leading edge's angular velocity shows large gradients. The rotation at maximal amplitude takes place in ¼ the time of the rotation at minimal amplitude. A minimal value of -1.7 N lift force is attained during the middle of rotation at minimal amplitude. At 1/4 of the way into the isolated rotation an absolute minimum in lift force is attained. Although the rotational phases differ in time length, negative forces are generated over a similar time span.

3.3 Flow field

PIV measurements were performed at various phases of the flapping cycle, where the force measurements labeled in figure 5 were performed and the wings were positioned as indicated by the red-colored sections in figure 4. Figure 6 shows the in-plane velocity component of the 3D vector field obtained by stereoscopic PIV measurements at these time instants, with the measurements made at the ¾ spanwise position. The color-contours indicate the magnitude of the vertical velocity component, to assist the interpretation of vortical motion as well as of momentum flux in relation to

vertical force. The black-colored regions represent the areas were data are compromised due to stray laser light reflections.

The first situation, represented in figure 6A, corresponds to the moment when the trailing edges separate at the end of the peel. Around the leading edges a swirl of air into the gap, identified as leading edge vortices, can be clearly distinguished. This outstroke leading edge vortex is indicated in figure 6 with OLV (prefixes O and I are used to distinguish flow features created during outstroke and instroke, respectively). Ellington [8] describes the leading edge vortex as a separation bubble, appearing on a sharp leading edge accelerating at a high angle of attack, which adds circulation to the wing's bound vortex and thus increases lift.

When the point of contact between the two wings reaches the trailing edges the end of the clap phase is reached. A vortex is visible near both trailing edges (figure 6A). These vortices are in the opposite direction of the expected stopping vortex. Most probably the air expelled by the clap rolls up into a jet vortex (JV). Whether the stopping vortices are eliminated by the presence of the mirror wing, as suggested by Weis-Fogh [7], or counteracted by the jet vortices is unknown. Since the jet vortices are in the same direction as the bound circulation of the subsequent translational stroke, they do not hinder the buildup of circulation according to the Wagner effect [9]. The high peak value in lift force attained in the first part of the outstroke (figure 5) indicates that the peel mechanism is very effective in lift generation.

Halfway through the outstroke (figure 6B), an influx of flow from above the wings fills the complete opening formed between the separating wings, corresponding to Weis Fogh's theory. However, in opposition to this theory a starting vortex (OSV) is shed from both trailing edges after they have separated. Whether the leading edge vortex is still present cannot be assessed unambiguously from the PIV result because of the poor accuracy near the wings, but is doubtful since the inrush of air decreases the angle of attack considerably and the lift force steadily decreases (figure 5).

At the end of the outward motion the leading edges slow down and the angles of attack increase until the wings are positioned almost vertically. The leading edge then rotates backwards relative to the translation. The rotational and translational velocity amount to a higher velocity above than below the wing and an upward lift force is generated. Although a peak in lift force is expected due to this Magnus effect [11], the lift decreases considerably and reaches negative values before rotation at the maximal stroke angle in this experiment. The drop in lift is supposedly attributed to the diminishing downwash, the reaction force on the abrupt upward motion of the leading edges (figure 4) and the starting vortex travelling slowly into the wake and counteracting the buildup of bound circulation (figure 6C).

Subsequently the wing flexes: the upper part of the wings rotate, while the trailing edges stay almost stationary (figure 6C-D). Unlike the theory of the flex mechanism, the formation of a leading edge vortex cannot be inferred from the PIV results. The PIV measurement in the region where the vortex is supposed to appear is obstructed by the shadow from the leading edge spar and the reflections on the wing foil. However, the lift force steadily increases and therefore it is expected that the leading edge vortex does exist. The downward leading edge motion during peel might reinforce the leading edge vortex generation by increasing the velocity of the fluid moving into the opening gap.

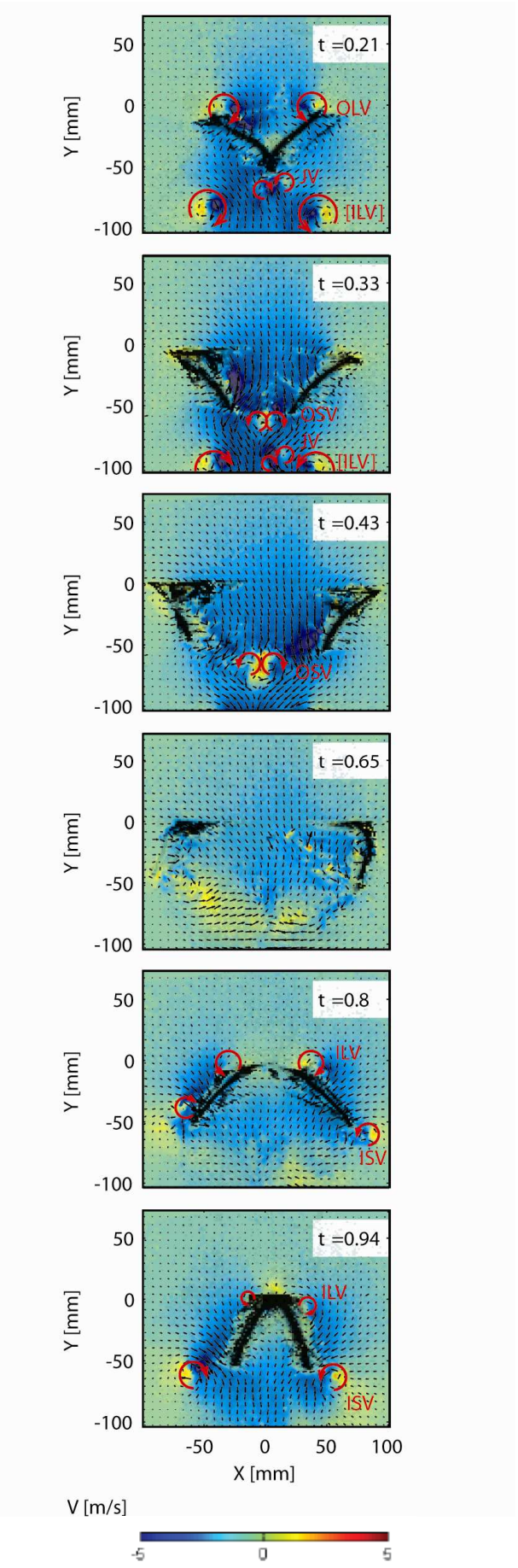

Figure 6: PIV results. *Color contours indicate the vertical velocity component. Unreliable areas affected by strong laser light reflections have been shaded for clarity. Frames a to f correspond to the different phases in the flapping cycle identified in fig. 4 and 5.*

Subsequently the leading edges accelerate towards the neutral position, the wing foils unflex and the angle of attack is highest (figure 6E). These conditions correspond to the conditions necessary for the generation of a separation bubble as described by Ellington [8]. At this moment the instroke leading edge vortex (ILV) can first be distinguished on the PIV images at ¾ span. A combined start and stop vortex is shed at the trailing edge (ISV). No wake recapture [11] has been visualized.

In the initial part of the clap (figure 6F), the leading edges come together and the angle of attack decreases until the wings are positioned almost parallel to one other. In contrary to Weis-Fogh's [7] suggestion, no expelling downward jet could be observed during the largest part of the clap at ¾ span. This is attributed to the high flexibility of the wing foil. Air is being expelled upward from the clapping leading edges, contributing negatively to the lift force, and the leading edges flex upward inducing a negative reaction force. Since the lift force attains a second minimum, the force generated by the downward jet is seemingly insufficient to overcome the negative contribution of the upward jet and the reaction force to the upward motion of the leading edges (figure 5).

The starting vortex slowly moves downstream into the wake. In figure 6A and 6B, the instroke starting vortex of the previous cycle is indicated with square brackets. Before the clap has been completed the leading edges have already started separating again and the wings curve toward the opposite side and the surfaces peel apart.

4 CONCLUSION

PIV velocity measurements and simultaneous force measurements were performed on the DelFly II flapping-wing MAV, to investigate the flow-field behavior and the aerodynamic force generated.

The wings deform considerably during the course of a flapping cycle due to the interaction of aerodynamic, inertial and elastic forces. A flex motion at the point of the isolated rotation and a figure-of-eight shaped leading edge heaving motion, as generally described for insect's wing kinematics can be clearly recognized. The wings clap and fling under high deformation and these two motions overlap one other in time.

In the early part of the clap, lift is rather attenuated before being enhanced, due to an upwardly expelled jet between the approaching leading edges. In the peel phase the PIV analysis shows a strong influx between the wings and a vortex structure above the leading edges. This peel mechanism contributes significantly to the lift, as revealed by the force measurements. At the end of the clap, the presence of a mirror wing causes the air to be expelled downward and to roll up into vortices of the same direction as the bound vorticity of the subsequent stroke.

The LEV generated during the peel stays attached to the wing surface in the beginning of the outstroke, producing a high peak force that is found at 1/3 of the way into the outstroke. The strong and chaotic starting vortex shed at the beginning of the outstroke is responsible for the subsequent strong decline in lift force during the last part of the translational phase.

The occurrence of a leading edge vortex during the flex cannot be assessed from the PIV images due to optical obstruction, but is likely to appear since the wing flexing is accompanied with a large increase in lift. An additional augmentation in lift could also be attained by the delayed shedding of a combined starting and stopping vortex. Although this flap phase is accompanied by an increased lift, it does not contribute to the total lift as much as the peel mechanism.

The PIV visualization first suggests the occurrence of a leading edge vortex at the onset of the subsequent translational stroke. The increase in lift force is prolonged until 2/3 of the way into the instroke.

The results of this study reveal that the most important augmentation in lift generation is due to the peel motion in the current wing configuration of DelFly II. Another significant contribution possibly is the combined vortex shedding and leading edge vortex strengthening at isolated wing rotation.

REFERENCES

[1] S.P. Sane. The aerodynamics of insect flight. *J. Exp. Biol.,* 206: 4191-4208,2003

[2] F-O. Lehmann. The mechanisms of lift enhancement in insect flight. *Naturwissenschaften.* 91:101-122, 2004

[3] G.C.H.E. de Croon, K.M.E. De Clercq, R. Ruijsink, B. Remes and C. de Wagter. Design, aerodynamics and vision-based control of the DelFly. *IJMAV,* submitted for publication

[4] C.P. Ellington. The novel aerodynamics of insect flight: applications to micro-air vehicles. *J. Exp. Biol.,* 202:3439-3448, 1999.

[5] K.M.E. De Clercq, R. de Kat, B. Remes, B.W. van Oudheusden en H. Bijl. Flow visualization and force measurements on a hovering flapping-wing MAV 'DelFly II'. *AIAA* , submitted for publication

[6] A.M. Mountcastle and T.L. Daniel. Aerodynamic and functional consequences of wing compliance. *Exp. Fluids* DOI 10.1007/s00348-008-0607-0, 2008

[7] T. Weis-Fogh. Quick estimates of flight fitness in hovering animals, including novel mechanisms for lift production. *J. Exp. Biol.,* 59:169-230, 1973

[8] C.P. Ellington. The aerodynamics of hovering insect flight IV Aerodynamic mechanisms. *Phil. Trans. R. Soc. Lond.* 305:79-113,1984

[9] P.B. Walker. Experiments on the growth of circulation about a wing and an apparatus for measuring fluid motion. *Rep. Memo. Aeronaut. Res. (Great Britain)* No 1402, 1931

[10] M.F.M. Osborne. Aerodynamics of flapping flight with application to insects. *J. Exp. Biol.,* 28:221-245, 1951.

[11] M.H. Dickinson, F-O Lehmann and S.P. Sane. Wing rotation and the aerodynamic basis of insect flight. S*cience*, 284:1954-1960, 1999

[12]

[13] F-O. Lehmann. The mechanisms of lift enhancement in insect flight. *Naturwissenschaften.* 91:101-122, 2004

[14] Ellington,C.P. The aerodynamics of hovering insect flight. III. Kinematics. *Phil. Trans. R. Soc. Lond.* B 305, 79-113, 1984